

Vibrational Phenomena in Glasses at Low Temperatures Captured by Field Theory of Disordered Harmonic Oscillators

Florian Vogel[✉] and Matthias Fuchs[✉]
 University of Konstanz—D-78457 Konstanz, Germany

 (Received 20 November 2022; accepted 4 May 2023; published 7 June 2023)

We investigate the vibrational properties of topologically disordered materials by analytically studying particles that harmonically oscillate around random positions. Exploiting classical field theory in the thermodynamic limit at $T = 0$, we build up a self-consistent model by analyzing the Hessian utilizing Euclidean random matrix theory. In accordance with earlier findings [T. S. Grigera *et al.* *J. Stat. Mech.* (2011) P02015.], we take nonplanar diagrams into account to correctly address multiple local scattering events. By doing so, we end up with a first principles theory that can predict the main anomalies of athermal disordered materials, including the boson peak, sound softening, and Rayleigh damping of sound. In the vibrational density of states, the sound modes lead to Debye's law for small frequencies. Additionally, an excess appears in the density of states starting as ω^4 in the low frequency limit, which is attributed to (quasi-) localized modes.

DOI: 10.1103/PhysRevLett.130.236101

Introduction.—The athermal excitations in glasses differ characteristically from the ones in ordered systems of the same chemical substances. While the vibrational properties of crystalline solids are well understood in terms of phonons, viz. wavelike small particle displacements from lattice positions, the vibrational spectra of amorphous solids exhibit incompletely understood anomalies.

One usually names three phenomena [1]. (i) Whereas the Debye law holds in crystalline solids in the low energy regime, there appears a maximum in the reduced vibrational density of states (VDOS) $[g(\omega)/\omega^2]$ in amorphous solids [1–5]. This maximum is referred to as the *boson peak*, where ω is the frequency. (ii) Experimental and computational data suggest that the sound attenuation results from disorder scattering and is Rayleigh-like $\propto p^4$ below the boson peak, where p is the wave vector. When entering the frequency regime of the boson peak the damping turns into a p^2 law [4,6–12] which is additionally indicated by a (iii) softening of the sound velocity, i.e., a dip in the reduced dispersion relation around the frequency of the boson peak [6,7,13]. It has been conjectured that these phenomena are interrelated and that they are connected to quasilocalized modes (QLMs) [8,10,13–17]. QLMs have been found in many computer simulations of disordered materials. It was also demonstrated that their density of states follows a universal $\propto \omega^4$ law and that they hybridize with phonons, so that neither of the two modes are exact eigenvectors of the dynamical matrix anymore, which is constituted by the Hessian of the potential energy [10,17,18].

The localization of modes in amorphous systems and the resulting fluctuations of elastic constants is at the heart of many prominent models, such as the two-level system [19], the soft potential model [20–22] and its generalizations [23], mean field approaches [5,24], and the heterogeneous

elasticity theory (HET) [8,13,16]. Nevertheless, all these approaches require phenomenological parameters and they generally do not capture the vibrational anomalies starting from the microscopic laws of motion. For example, the widely used HET [8,13,16] is a mesoscopic rather than a microscopic theory which quantitatively underestimates the importance of QLMs [14,15,25].

In this Letter, we start from the microscopic equations of disordered coupled harmonic oscillators. This approach leads to the Euclidean random matrix (ERM) problem suggested by Parisi and co-workers [2,26,27]. Following them, we rely on a Green's function formalism to derive a self-consistent model that rationalizes all aforementioned anomalies and thus improves on earlier ERM models. The guiding principle in our derivation is that multiple local scattering events are of qualitative importance [28]. This is also hinted at by the discovered influence of nonplanar diagrams [29,30], which were identified as origin of Rayleigh damping in the ERM [31–33]. Therefore, we develop a model that relies on a vertex instead of propagator renormalization.

The system.—We study a system of N particles randomly placed in a volume V at the positions $\{\mathbf{r}_i\}^N$ in the thermodynamic limit with N/V being constant. The positions are drawn from a uniform distribution $P\{\{\mathbf{r}_i\}^N\} = 1/V^N$. Considering small fluctuations ϕ_i around the frozen positions \mathbf{r}_i , we define the symmetric random matrix \mathbf{M} via the second derivative of an interaction pair potential $U(\{\phi_i\}) = \frac{1}{2} \sum_{i,j=1}^N f(\mathbf{r}_i - \mathbf{r}_j)(\phi_i - \phi_j)^2 = \sum_{i,j} M_{ij} \phi_i \phi_j$. The f is a spring function which quantifies the interaction strength. We only request for the theoretical investigation that the Fourier transformation $\hat{f}(\mathbf{p})$ exists. We also assume rotational invariance, so that \hat{f} only depends on the absolute

modulus of the wave vector $p = |\mathbf{p}|$ and that the spring function is regular. This implies $\hat{f}(\mathbf{0}) - \hat{f}(\mathbf{p}) \propto p^2$ for small \mathbf{p} . When performing numerical calculations, we set $\hat{f}(\mathbf{p}) = (2\pi\sigma^2)^{3/2} e^{-\sigma^2 p^2/2}$. Here, σ is an intrinsic length scale of the system, which leads to a dimensionless density $n = N\sigma^3/V$. The density n turns out to be the single state parameter. In the following, σ will be set to unity. Note, that we neglect the vector character of ϕ . The scalar ϕ_s represent transverse displacements, which predominantly contribute to the boson peak [34].

The fundamental equations of motion of N coupled harmonic oscillators read

$$\ddot{\phi}_i = - \sum_{j=1}^N M_{ij} \phi_j, \quad \text{for } 1 \leq i \leq N. \quad (1)$$

Here, time and (later) frequency are made dimensionless by a frequency scale ω_0 (set to $\omega_0 = 1$ for simplicity) that can be taken from the position of the boson peak in measurements. Translational invariance and hence momentum conservation follow immediately from the potential $U(\{\phi_i\})$. Consequently, \mathbf{M} has the eigenvalue zero. The associated eigenvector \mathbf{e}_0 corresponds to the uniform shift $\mathbf{e}_0 = (1, 1, \dots, 1)$. For positive spring function, the potential U is positive and thus the matrix \mathbf{M} is semipositive definite.

It is noteworthy that the disorder in \mathbf{M} and the thermodynamic limit lead to a broadening of the oscillator lines in the dynamic structure factor and to sound attenuation, even though the eigenvalues of the matrix \mathbf{M} are exclusively non-negative and thus the oscillator frequencies real. We interpret this as a instantiation of Landau damping [35]: in time-reversible equations of motion and in the thermodynamic limit, damping can arise from energy transfer among the infinite multitude of modes.

We study the ERM system by analyzing the two-point response or Green's function G . It gives the evolution of an initial displacement field with plane wave form of wave vector \mathbf{p} . $G(\mathbf{p}, z)$ is its spectrum at eigenvalue z and is related to the resolvent of \mathbf{M}

$$G(\mathbf{p}, z) = \lim_{N, V \rightarrow \infty} \frac{1}{V} \overline{\sum_{i,j=1}^N e^{i\mathbf{p} \cdot (\mathbf{r}_i - \mathbf{r}_j)} \left[\frac{1}{z - \mathbf{M}} \right]_{ij}}. \quad (2)$$

Here, $z = (\omega + i0^+)^2 \in \mathbb{C}$ with ω corresponding to the frequency. The overline indicates the sample average over the disorder. The resolvent can be connected to observables like the dynamic structure factor and the density of states [2,26,36]. See Supplemental Material (SM), Sec. II [37], for further information.

Self-consistent model.—Following [2,27,30], we perform a high density expansion of the resolvent (2). Using the Dyson equation, $G = G_0 + G_0 \Sigma G$, we express the Green's function in terms of a bare propagator

$G_0(\mathbf{p}, z) = [z/n - \epsilon_0(\mathbf{p})]^{-1}$ and the self-energy $\Sigma(\mathbf{p}, z)$, with $\epsilon_0(\mathbf{p}) = \hat{f}(\mathbf{0}) - \hat{f}(\mathbf{p})$ giving the bare dispersion relation. While G_0 describes undamped harmonic oscillators, Σ arises from the disorder in the elastic couplings. We envision a perturbation traveling through the system, and consider the field ϕ_i as excitation at the respective lattice site so that the interaction between the perturbation and the disorder can be called scattering event [30]. The self-energy thus contains all the inelastic scattering events. Σ has a series expansion in $(1/n)$ and vanishes for $n \rightarrow \infty$, where the disorder vanishes. Thus, $1/n$ quantifies the disorder and the weakening of the elastic constants $f(\mathbf{r}_i - \mathbf{r}_j)$ when the separation of particles gets larger. Using Feynman diagrams, we reconstruct the different inelastic scattering processes. Since this approach has been tried before [2,27,30], we moved further comments on the technical details to SM, Sec. I [37].

The derivation of our self-consistent model starts with the insight that any contribution to the self-energy necessarily ends with the same vertex and that the momentum is conserved at every vertex. This allows us to write down the self-energy schematically:

$$\Sigma(\mathbf{p}, z) = \begin{array}{c} \text{[Diagram: A square vertex connected to a curly line loop]} \\ \text{[Diagram: A square vertex connected to a curly line loop with a circle vertex]} \\ \text{[Diagram: A square vertex connected to a curly line loop with two circle vertices labeled A and B]} \\ \text{[Diagram: A square vertex connected to a curly line loop with three circle vertices labeled A, B, and C]} \\ \dots \end{array} \quad (3)$$

Here, a straight line represents the bare propagator; a curly line a density fluctuation, and the circle denotes a vertex and marks an inelastic scattering event. The square can be regarded as a renormalized vertex [38], which absorbs all possible insertions at a bare vertex. The letters A, B, C just label the different building blocks in (3) which are of second order in density fluctuation. The three dots represent more diagrams with more simultaneous density fluctuations. Every new loop comes with an additional factor $1/n$. Thus, one can truncate the expansion after a few orders in the high density limit.

A self-consistent model is easily constructed by only keeping classes of diagrams with the topologies A, B , and C and, in the lower line of Eq. (3), by replacing the bare propagator between two bare vertices with the full Green's function $G(\mathbf{p}, z)$. (Note, a dressed Green's function ending in a renormalized vertex would lead to an overcounting. This can be easily seen by inserting the Dyson equation.) In contrast to earlier models [2,33,39], this resummation takes all the diagrams that topologically match the ones from second order perturbation theory and hence nonplanar diagrams into account. We do this for two related reasons: (i) QLMs are arguably important for the modes of vibrations of low temperature glasses [14,15,17,40] and one must therefore correctly consider multiple local scattering

events. Planar diagrams underestimate these scattering sequences [14,15,28]. (ii) Nonplanar diagrams are needed to give the correct Rayleigh damping of sound modes for $p \rightarrow 0$ and to prevent a potential infrared divergence of the self-energy [29,41]. The Feynman rules stated in SM, Sec. I [37], allow us to write down the associated amplitude for our self-consistent model

$$G(\mathbf{p}, z) = \frac{1}{z/n - \epsilon_0(\mathbf{p}) - \Sigma(\mathbf{p}, z)}, \quad (4a)$$

$$\Sigma(\mathbf{p}, z) = \int \frac{d^3 \mathbf{k}}{(2\pi)^3} V(\mathbf{k}, \mathbf{p}) \mathcal{V}(\mathbf{k}, \mathbf{p}, z), \quad (4b)$$

$$\begin{aligned} & \left[nG_0^{-1}(\mathbf{k}, z) - \int \frac{d^3 \mathbf{q}}{(2\pi)^3} V^2(\mathbf{q}, \mathbf{k}) G(\mathbf{q}, z) \right] \mathcal{V}(\mathbf{k}, \mathbf{p}, z) \\ &= V(\mathbf{k}, \mathbf{p}) + \int \frac{d^3 \mathbf{q}}{(2\pi)^3} [V(\mathbf{q} - \mathbf{k}, 2\mathbf{q} - \mathbf{p}) + V(\mathbf{p} - \mathbf{q}, \mathbf{k}) \\ & \quad \times G(|\mathbf{p} - \mathbf{k} - \mathbf{q}|, z) V(\mathbf{p} - \mathbf{k}, \mathbf{q})] \mathcal{V}(\mathbf{q}, \mathbf{p}, z), \end{aligned} \quad (4c)$$

$$V(\mathbf{k}, \mathbf{p}) = \hat{f}(\mathbf{k}) - \hat{f}(\mathbf{k} - \mathbf{p}) = -V(\mathbf{p} - \mathbf{k}, \mathbf{p}). \quad (4d)$$

While one could easily include more diagrams, there is no need for it. On the contrary, we will now argue that this minimal model successfully captures all the vibrational phenomena of low temperature glasses. Importantly, we consider stable glass states while previous approaches had considered marginally stable glasses where a close-by instability leads to vibrational anomalies [2,39,42].

Results.—(a) Dispersion relation: The dispersion relation $\epsilon(\mathbf{p}) = n(\epsilon_0(\mathbf{p}) + \text{Re}[\Sigma(\mathbf{p}, z = 0)])$ characterizes the peak positions of the vibrational modes in the dynamic structure factor; it is shown in Fig. 1. The limiting proportionality $\epsilon(p) \propto n$ for $n \rightarrow \infty$ arises from the pairwise interaction among all particles. The expansion $\epsilon(\mathbf{p} \rightarrow 0) \rightarrow (c_T p)^2$ indicates the presence of sound waves in the hydrodynamic limit. They are expected as Goldstone modes arising from broken translational invariance. Here, c_T is the (transverse) speed of sound. Lowering the density increases the disorder and weakens the elasticity; the frequencies of vibrations become softer. Additionally, a dip appears around $\sigma p \approx 10$. This indicates a negative dispersion of the sound velocity, i.e., sound softening, and also suggests the presence of the boson peak in the VDOS [6,7,13]. For very small n , $\epsilon(p \approx 10/\sigma)$ may become negative, but this density range is not considered. Considering only diagrams of type A in Eq. (3), a self-consistent resummation of all planar diagrams is possible [2,39], which for reference is presented in SM, Sec. V [37]. It captures wave modes equally well and gives comparable results for $\epsilon(p)$ as included in Fig. 1.

(b) Sound attenuation: The sound attenuation is given by the imaginary part of the self-energy. It determines the

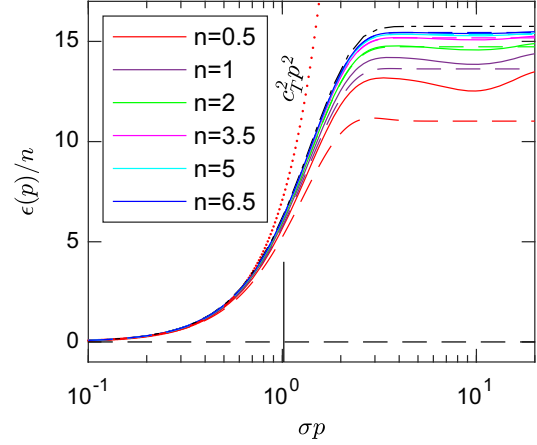
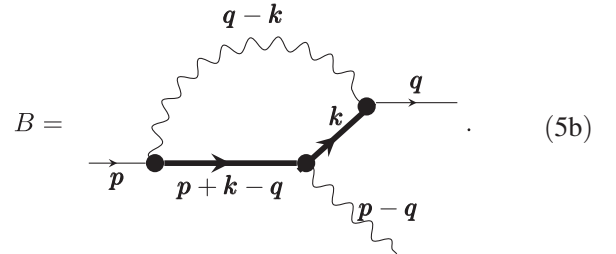
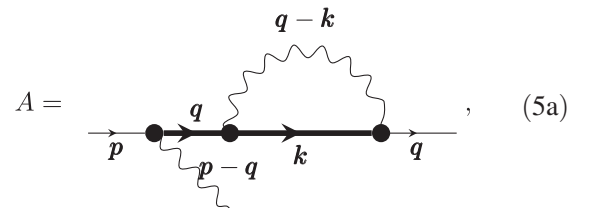


FIG. 1. The reduced dispersion relation $\epsilon(p)/n$ (solid lines) is shown for different densities as a function of wave vector p . It is compared to the associated bare dispersion $\epsilon_0(p)$ (dash-dotted line) and to the result from the planar resummation (dashed lines) [39]. The limit of sound propagation, $\epsilon(p \rightarrow 0) \rightarrow (c_T p)^2$ is indicated for $n = 0.5$. At this n , the vertical bar marks $p_{BP} = \omega_{BP}/c_T$, the wave number delimiting the sound behavior.

width of the vibrational mode around the sound pole. The self-consistent resummation of the planar diagrams alone [2,30,39] leads to strong hydrodynamic sound damping (viz. $\propto p^2$), while experiments [6,12] and simulations [7,14,43] indicate weaker Rayleigh damping (viz. $\propto p^4$). It can be understood to result from wave scattering off the frozen disorder. To show that the nonplanar diagrams fix the error of a planar self-consistent approach, we argue that the imaginary parts of the planar diagrams [class A, first line in Eq. (4c) and given in diagram (5a)] and nonplanar diagrams [class B, last line in Eq. (4c) and given in diagram (5b)] cancel each other exactly for $p \rightarrow 0$.



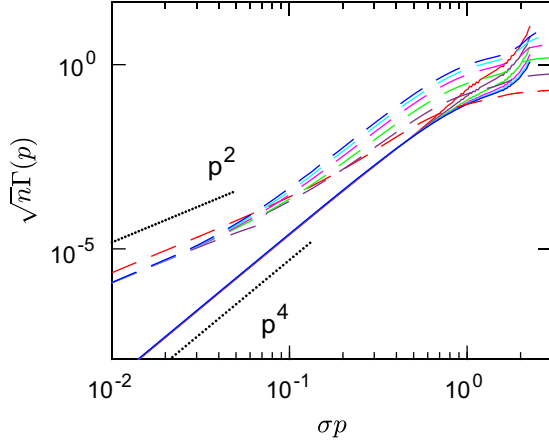


FIG. 2. Sound attenuation as function of wave vector p . Rescaled data $\sqrt{n}\Gamma(p)$ collapse for high densities n (see legend in Fig. 1) for small p . Solid lines follow from the imaginary part of the self-energy given by Eq. (4), dashed lines follow from planar diagrams [39] (see SM [37]). The sound attenuation is calculated around the sound pole $\omega = \sqrt{\epsilon_0(p)}$. Dotted lines represent asymptotic power laws.

The thick line represents the full Green's function. Both diagrams describe equivalent scattering processes off two density fluctuations but in different sequence. The cancellation can be seen by applying the Sokhotski-Plemelj identity $[x \pm i0^\pm]^{-1} = \mp i\pi\delta(x) + \mathcal{P}(1/x)$ to the full propagator in the hydrodynamic limit and by integrating over \mathbf{k} ; here, \mathcal{P} represents the Cauchy-principal value. For small p , the symmetry (4d) gives the cancellation; see proof in SM [37], Sec. III. It also fixes the infrared divergence problem [29,41]. The building block containing the four vertex [diagram C in (S5) in SM [37]] gives the correct imaginary part by itself. In total, this leads to $G(\mathbf{p}, z)/n = [z - \epsilon(\mathbf{p}) - i\omega(\mathbf{p})\Gamma(\mathbf{p})]^{-1}$ with $\Gamma(\mathbf{p}) = n\text{Im}\Sigma(\mathbf{p}, z = \epsilon(\mathbf{p}))/\omega(\mathbf{p}) = B_R p^4$ around the sound pole $\omega(\mathbf{p}) = \sqrt{\epsilon(\mathbf{p})}$ in the hydrodynamic limit. The strength of Rayleigh damping B_R increases with disorder.

Figure 2 shows the sound attenuation for different densities in the two loop approximation; see SM [37] for details. Since our full model (4) topologically coincides with the second order, the second order solution confirms that (4) predicts the correct sound attenuation.

(c) Vibrational density of states: The VDOS can be calculated from the large wave-vector limit of the Green's function where only diagonal elements of \mathbf{M} contribute in Eq. (2) [2,27]; see SM, Sec. IV, for details [37]. The sound modes already identified in the dispersion relation suggest that the VDOS contains a Debye spectrum $g_D(\omega) = \omega^2/\omega_D^3$ for $\omega \rightarrow 0$. The Debye frequency ω_D characterizes the region of long-wavelength sound and gives an upper cutoff for waves in solids. It shrinks with increasing disorder and the magnitude of the Debye law increases for decreasing n ; see panel (a) in Fig. 3. Note, that panel (a) has been

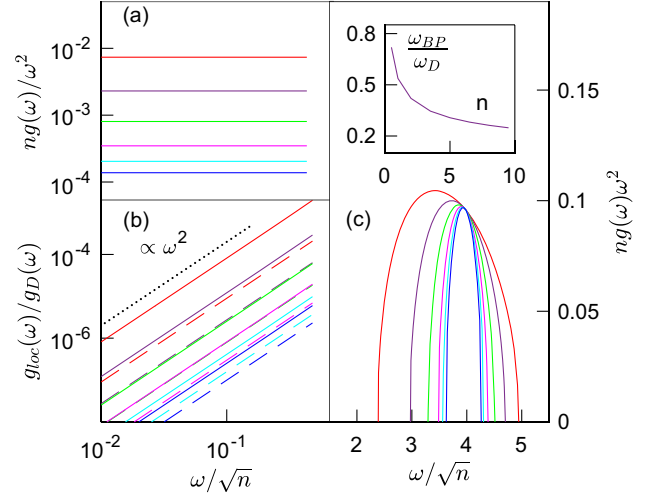


FIG. 3. Panel (a), full lines show the reduced vibrational density of states (VDOS), $ng(\omega)/\omega^2$, for low frequencies at different number densities n . Panel (b) presents the VDOS of the quasilocalized modes (QLM), $g_{\text{loc}}(\omega)/g_D(\omega)$, where the dashed line shows the prediction of the HET theory. Panel (c) exhibits the rescaled boson peak, $ng(\omega)/\omega^2$, which is located at the upper end of the dispersion relation. The inset shows the ratio ω_{BP}/ω_D of boson peak and Debye frequencies. The densities and their respective colors are the same in all three panels following the legend in Fig. 1.

calculated under the assumption that ω^2 is small; see SM, Sec. IV [37]. This approximation breaks down for $\omega \rightarrow 1$. The boson peak is situated at the upper end of the spectrum of vibrations in the model. There, the VDOS can be simplified as the contributions of the acoustic phonons to the self-energy become weak. This leads to a closed expression for the VDOS which is Wigner's semicircle law as expected in uncorrelated random matrix ensembles [5,36,44]. The amplitude of the boson peak shown in panel (c) of Fig. 3 only varies little with increasing disorder, while its position shifts trivially with \sqrt{n} . The ratio of its position to the Debye frequency, ω_{BP}/ω_D [see the inset in panel (c) of Fig. 3], is smaller as one indicating that ω_{BP} , and not ω_D , sets the limit for wave behavior in random matrix approaches [13,45]. In simulations of stable glasses [46], the boson peak lies low, $\omega_D/\omega_{BP} \approx 6$.

(d) Quasilocalized modes: Recent works [8,14,17,46] established a close relation between QLMs and Rayleigh damping by showing that there is a linear relation between the damping coefficient B_R and the coefficient A_4 of the characteristic VDOS of the quasilocalized modes $g_{\text{loc}} = A_4\omega^4$. Additionally, it was argued in [47] that the presence of QLMs implies a p^4 sound attenuation. Furthermore, it has been shown that QLMs give rise to the boson peak [1,10,14,17,22]. This suggests that QLMs are at the heart of the vibrational anomalies of disordered materials. Our results in Figs. 2 and 3 support this narrative. In finite systems, the participation ratio can be used to

identify QLMs, which is impossible here as the thermodynamic limit was taken. Thus, we interpret the QLMs as the modes that have a VDOS proportional to the Rayleigh term B_R . We show the quartic contribution to the VDOS in panel (b) of Fig. 3, again utilizing a small ω approximation. We also compare it to the HET prediction $g_{\text{loc}}^{\text{HET}}/\omega^4 = 2B_R/(\pi\omega_D^2c_T^4)$ [8,10], which underestimates disorder in stable glasses quantitatively [14,46], where $(c_T^4\omega_{BP}^2)A_A/B_R \approx 0.05$ holds; our ratio 0.045 for $n = 0.5$ lies close. The anomaly is missing in the VDOS of the self-consistent planar theory [2,39], which confirms that planar diagrams overly restrict the sequence of interactions of vibrational modes with particle sites; for details see SM, Sec. V [37].

Conclusion and outlook.—Our self-consistent field theory of ERM accounts for disorder more accurately than approaches based on mean field or coherent potential approximations. The latter underestimate multiple local scattering events, which become important if one has bound states or localization effects [28]. Neglecting dependent scattering processes in an ERM model leads to a planar theory for the VDOS in the thermodynamic limit [36]. This, together with the cancellation of diagrams in Eq. (5) to get the correct Rayleigh damping suggests that nonplanar diagrams are essential to correctly address disorder. Besides this qualitative insight, we constructed a self-consistent theory for disordered harmonic oscillators that correctly predicts all the vibrational anomalies of disordered materials. It can be coarse grained and then leads to the widely used HET. After understanding the topology of athermal disorder, the next step is to take the vector character of the displacement fields into account and to consider finite temperatures. Additionally, it would be worthwhile to relate the approach to the soft potential model and its generalizations.

We thank Matthias Krüger, Annette Zippelius, Thomas Franosch, and Walter Schirmacher for fruitful discussions. The work was supported by the Deutsche Forschungsgemeinschaft (DFG) via SFB 1432 Project No. CO7.

[1] A. Marruzzo, S. Köhler, A. Fratallocchi, G. Ruocco, and W. Schirmacher, Vibrational anomalies and marginal stability of glasses, *Eur. Phys. J. Spec. Top.* **216**, 83 (2013).
 [2] S. Ciliberti, T.S. Grigera, V. Martin-Mayor, G. Parisi, and P. Verrocchio, Brillouin and boson peaks in glasses from vector Euclidean random matrix theory, *J. Chem. Phys.* **119**, 8577 (2003).
 [3] J. Wuttke, W. Petry, G. Coddens, and F. Fujara, Fast dynamics of glass-forming glycerol, *Phys. Rev. E* **52**, 4026 (1995).
 [4] G. Baldi, V.M. Giordano, G. Monaco, and B. Ruta, Sound Attenuation at Terahertz Frequencies and the Boson Peak of Vitreous Ailica, *Phys. Rev. Lett.* **104**, 195501 (2010).

[5] S. Franz, G. Parisi, P. Urbani, and F. Zamponi, Universal spectrum of normal modes in low-temperature glasses, *Proc. Natl. Acad. Sci. U.S.A.* **112**, 14539 (2015).
 [6] G. Monaco and V. Giordano, Breakdown of the Debye approximation for the acoustic modes with nanometric wavelengths in glasses, *Proc. Natl. Acad. Sci. U.S.A.* **106**, 3659 (2009).
 [7] G. Monaco and S. Mossa, Anomalous properties of the acoustic excitations in glasses on the mesoscopic length scale, *Proc. Natl. Acad. Sci. U.S.A.* **106**, 16907 (2009).
 [8] W. Schirmacher, G. Ruocco, and T. Scopigno, Acoustic Attenuation in Glasses and Its Relation with the Boson Peak, *Phys. Rev. Lett.* **98**, 025501 (2007).
 [9] A. Marruzzo, W. Schirmacher, A. Fratallocchi, and G. Ruocco, Heterogeneous shear elasticity of glasses: The origin of the boson peak, *Sci. Rep.* **3**, 1407 (2013).
 [10] H. Mizuno and A. Ikeda, Phonon transport and vibrational excitations in amorphous solids, *Phys. Rev. E* **98**, 062612 (2018).
 [11] G. Baldi, V.M. Giordano, B. Ruta, R. Dal Maschio, A. Fontana, and G. Monaco, Anharmonic Damping of Terahertz Acoustic Waves in a Network Glass and Its Effect on the Density of Vibrational States, *Phys. Rev. Lett.* **112**, 125502 (2014).
 [12] G. Baldi, M. Zanatta, E. Gilioli, V. Milman, K. Refson, B. Wehinger, B. Winkler, A. Fontana, and G. Monaco, Emergence of Crystal-like Atomic Dynamics in Glasses at the Nanometer Scale, *Phys. Rev. Lett.* **110**, 185503 (2013).
 [13] W. Schirmacher and G. Ruocco, Heterogeneous elasticity: The tale of the boson peak, [arXiv:2009.05970](https://arxiv.org/abs/2009.05970).
 [14] L. Wang, L. Berthier, E. Flenner, P. Guan, and G. Szamel, Sound attenuation in stable glasses, *Soft Matter* **15**, 7018 (2019).
 [15] G. Szamel and E. Flenner, Microscopic analysis of sound attenuation in low-temperature amorphous solids reveals quantitative importance of non-affine effects, *J. Chem. Phys.* **156**, 144502 (2022).
 [16] S. Mahajan and M. P. Ciamarra, Unifying Description of the Vibrational Anomalies of Amorphous Materials, *Phys. Rev. Lett.* **127**, 215504 (2021).
 [17] E. Lerner and E. Bouchbinder, Low-energy quasilocalized excitations in structural glasses, *J. Chem. Phys.* **155**, 200901 (2021).
 [18] D. Richard, K. González-López, G. Kapteijns, R. Pater, T. Vaknin, E. Bouchbinder, and E. Lerner, Universality of the Nonphononic Vibrational Spectrum across Different Classes of Computer Glasses, *Phys. Rev. Lett.* **125**, 085502 (2020).
 [19] P. W. Anderson, B. I. Halperin, and C. M. Varma, Anomalous low-temperature thermal properties of glasses and spin glasses, *Philos. Mag. A* **25**, 1 (1972).
 [20] Yu. M. Galperin, V. G. Karpov, and V. I. Kozub, Localized states in glasses, *Adv. Phys.* **38**, 669 (1989).
 [21] D. A. Parshin, Soft potential model and universal properties of glasses, *Phys. Scr.* **T49A**, 180 (1993).
 [22] D. A. Parshin, H. Schober, and Yu. M. Gurevich, Vibrational instability, two-level systems, and the boson peak in glasses, *Phys. Rev. B* **76**, 064206 (2007).
 [23] E. Bouchbinder, E. Lerner, C. Rainone, P. Urbani, and F. Zamponi, Low-frequency vibrational spectrum of mean-field disordered systems, *Phys. Rev. B* **103**, 174202 (2021).

- [24] E. DeGiuli, A. Laversanne-Finot, G. Düring, E. Lerner, and M. Wyart, Effects of coordination and pressure on sound attenuation, boson peak and elasticity in amorphous solids, *Soft Matter* **10**, 5628 (2014).
- [25] C. Caroli and A. Lemaître, Fluctuating Elasticity Fails to Capture Anomalous Sound Scattering in Amorphous Solids, *Phys. Rev. Lett.* **123**, 055501 (2019).
- [26] M. Mézard, G. Parisi, and A. Zee, Spectra of Euclidean random matrices, *Nucl. Phys.* **559B**, 689 (1999).
- [27] V. Martin-Mayor, M. Mézard, G. Parisi, and P. Verrocchio, The dynamical structure factor in topologically disordered systems, *J. Chem. Phys.* **114**, 8068 (2001).
- [28] P. Sheng, *Introduction to Wave Scattering, Localization, and Mesoscopic Phenomena* (Elsevier Science, Amsterdam, 1995).
- [29] E. Leutheusser, Self-consistent kinetic theory for the Lorentz gas, *Phys. Rev. A* **28**, 1762 (1983).
- [30] T. S. Grigera, V. Martin-Mayor, G. Parisi, P. Urbani, and P. Verrocchio, On the high-density expansion for Euclidean random matrices, *J. Stat. Mech.* (2011) P02015.
- [31] C. Ganter and W. Schirmacher, Rayleigh scattering, long-time tails, and the harmonic spectrum of topologically disordered systems, *Phys. Rev. B* **82**, 094205 (2010).
- [32] C. Ganter and W. Schirmacher, Euclidean random matrix theory: Low-frequency non-analyticities and Rayleigh scattering, *Philos. Mag.* **91**, 1894 (2011).
- [33] W. Schirmacher, V. Folli, C. Ganter, and G. Ruocco, Self-consistent Euclidean-random-matrix theory, *J. Phys. A* **52**, 464002 (2019).
- [34] J. Horbach, W. Kob, and K. Binder, High frequency sound and the boson peak in amorphous silica, *Eur. Phys. J. B* **19**, 531 (2001).
- [35] C. Mouhot and C. Villani, On Landau damping, *Acta Math.* **207**, 29 (2011).
- [36] A. Goetschy and S. E. Skipetrov, Euclidean random matrices and their applications in physics, [arXiv:1303.2880](https://arxiv.org/abs/1303.2880).
- [37] See Supplemental Material at <http://link.aps.org/supplemental/10.1103/PhysRevLett.130.236101> for additional details on Feynman rules, analytical calculations, and a comparison with the planar theory.
- [38] A. K. Chattopadhyay, A. Basu, and J. K. Bhattacharjee, Coupled nonequilibrium growth equations: Self-consistent mode coupling using vertex renormalization, *Phys. Rev. E* **61**, 2086 (2000).
- [39] T. S. Grigera, V. Martín-Mayor, G. Parisi, and P. Verrocchio, Vibrational Spectrum of Topologically Disordered Systems, *Phys. Rev. Lett.* **87**, 085502 (2001).
- [40] H. R. Schober and G. Ruocco, Size effects and quasilocalized vibrations, *Philos. Mag.* **84**, 1361 (2004).
- [41] S. Schnyder, F. Höfling, T. Franosch, and Th. Voigtmann, Long-wavelength anomalies in the asymptotic behavior of mode-coupling theory, *J. Phys. Condens. Matter* **23**, 234121 (2011).
- [42] M. Shimada, H. Mizuno, and A. Ikeda, Vibrational spectrum derived from local mechanical response in disordered solids, *Soft Matter* **16**, 7279 (2020).
- [43] H. Mizuno, H. Shiba, and A. Ikeda, Continuum limit of the vibrational properties of amorphous solids, *Proc. Natl. Acad. Sci. U.S.A.* **114**, E9767 (2017).
- [44] W. Götze and M. R. Mayr, Evolution of vibrational excitations in glassy systems, *Phys. Rev. E* **61**, 587 (2000).
- [45] D. A. Conyuh and Y. M. Beltukov, Random matrix approach to the boson peak and Ioffe-Regel criterion in amorphous solids, *Phys. Rev. B* **103**, 104204 (2021).
- [46] L. Wang, A. Ninarello, P. Guan, L. Berthier, G. Szamel, and E. Flenner, Low-frequency vibrational modes of stable glasses, *Nat. Commun.* **10**, 26 (2019).
- [47] H. R. Schober, Quasi-localized vibrations and phonon damping in glasses, *J. Non-Cryst. Solids* **357**, 501 (2011).